

# Topographic Allocations of MmWave Access Points inside the Passenger Car of High Speed Trains

Feng Lu, Akira Yamaguchi, Kazunori Takeuchi, and Hiroyuki Shinbo  
KDDI Research, Inc. Fujimino, Saitama, 356-8502, Japan  
Email: {lu; yama; ka-takeuchi; shinbo}@kddi-research.jp

**Abstract**—Millimeter wave (mmWave) communication is one of the technologies to meet the ever increasing demand of high quality entertainment services inside the passenger car. In accordance with the gigabit class backhaul technology for the high speed trains, the target is to achieve gigabit class link throughput at almost all (99%) the seats inside the passenger car of high speed trains (PCoHST). However 60GHz band mmWave communication suffers from huge human blockage besides severer propagation loss than the 2.4GHz band, hence the area of gigabit class link throughput that one mmWave AP (MAP) can support is smaller. We have shown that at least 4 MAPs are necessary to meet the above target. This paper proposes two topographic allocation types for the 4 MAPs taking into account of the physical structure of the PCoHST, the propagation characteristics and human blockage in the mmWave band. We evaluate the allocation types by ray tracing simulations under 4 typical human blockage scenarios with 3 typical occupancy rates. Simulation results show that the straight in-line allocation type on the ceiling at the center of the vehicular width is more feasible.

**Index Terms**—Millimeter wave, IEEE802.11ad, mmWave access points, allocation passenger car, high speed train

## I. INTRODUCTION

Gigabit class communications in the passenger car of high speed trains (PCoHST) are expected for future railway communication so that the passengers can enjoy high quality video contents etc. [1]. Research works on gigabit class backhaul transmission technologies such as [1-2] have been published. In accordance with the gigabit class backhaul technologies, it is necessary to investigate gigabit class communications inside the PCoHST [3]. In this paper the target is to achieve gigabit class link throughput at almost all (99%) the seats inside the PCoHST.

MmWave systems such as IEEE802.11ad/WiGig [4] are promising to provide gigabit class communication. The design technologies of indoor Wireless LAN (WLANs, hereinafter referred to as Wi-Fi) have been established [5]. And the propagation characteristics of 2.2GHz, 2.4GHz as well as 5.2GHz band wireless system inside the PCoHST have been investigated [6]-[9]. However, these methods are not applicable to mmWave access point (MAP) deployment in the PCoHST because

in mmWave band, e.g., Channel 2 (60.48GHz) of WiGig, the propagation attenuation in free space is, about 28dB, higher than that of 2.4GHz band, and mmWave propagation can be easily blocked by obstructions including human bodies (the attenuation of human body is up to 35dB [10]), seats and luggage rack etc. compared to the lower frequency systems. The higher propagation loss and severer human blockage attenuation in mmWave band result in smaller coverage and severer performance degradation to the mmWave communication systems.

60GHz band systems initially operate in indoor, line-of-sight (LOS) domestic environments [11]. Since there are up to 100 seats inside the ordinary PCoHST [3], up to 100 MAPs are needed if only LOS paths are used for every seat. The more the number of MAPs, the more stable the mmWave communication between the MAP and the user terminal (UT(s)). On the other hand the more the number of MAPs, the higher the overall system cost and the severer the co-channel and inter-channel interference issues become. Therefore, it is important to determine the proper and minimal number of MAPs and find the topographic allocation types (TATs) for the MAPs in order to satisfy the mmWave coverage target in the PCoHST. We have shown in [12] that, with the introduction of beamforming antennas and in the human blockage scenarios that no person or only one person walking along the aisle in a fully occupied PCoHST, 4 is the minimal number of MAPs in order to satisfy the coverage target in the PCoHST. This paper deals with the remaining issue: where to deploy the 4 MAPs inside the PCoHST?

We propose two TATs and then compare the performance with 10 other possible TATs considering the physical structure of the PCoHST to achieve gigabit class link throughput target inside the PCoHST. All the TATs are evaluated under 4 typical human blockage scenarios with 3 typical occupancy rate by ray-tracing simulations. The propagation characteristics of mmWave band, obstruction of both standing and sitting human bodies, the LOS and non-line-of-sight (NLOS) relation between the UT and MAPs are taken into consideration.

The rest of this paper is organized as follows: Section II addresses the MAPs deployment issues in the PCoHST. Section III states the evaluation methods, TATs, human blockage scenarios and other simulation parameters. The simulations results and discussions are presented in Section IV. And finally, Section V concludes this paper.

---

Manuscript received November 15, 2018; revised July 8, 2019.  
This work was supported by the MIC of Japan.  
Corresponding author email: lu@kddi-research.jp.  
doi:10.12720/jcm.14.8.647-655

## II. MAPS DEPLOYMENT INSIDE THE PCOHST

### A. Definitions and Premises

The “coverage” of one MAP is defined as an area of seats in PCoHST where gigabit class link throughput is guaranteed. The “coverage rate” of all the MAPs in the PCoHST is defined as the ratio of the number of gigabit class link throughput achievable seats over the total number of seats in the PCoHST.

We have shown that 4 is the proper and minimal number of MAPs in order to achieve the at least 99% mmWave coverage rate target inside the PCoHST under two scenarios [12]. This is because when the number of MAPs is 3, there are 6 seats at which the received signal strength indicator (RSSI) from all the MAPs fall below -64dBm, the minimal RSSI level to achieve Gigabit level link throughput according to the IEEE 802.11ad standard [4]; and when the number of MAPs is 4, the RSSI at each of the 100 seats is not smaller than -64dBm. So the first premise is that the number of MAPs is 4. The second premise is that the antenna of both the MAPs and the UTs is high gain beamforming antenna with narrow beam width. The remaining issue is where to deploy the 4 MAPs with high gain antennas in order to meet the target coverage rate inside the PCoHST.

### B. Current Wi-Fi AP Deployment Methods and the Problems to Apply Them to MAPs Deployment.

As the relevant study of MAPs deployment, this section first introduces current Wi-Fi AP deployment methods, and then lists up several problems to apply them for MAPs deployment. The planning methods for indoor Wi-Fi have been established and were surveyed in [5]. The Wi-Fi deploy methods aim at selecting the locations for the reduced number of APs and their channel assignments while keeping low transmission power levels [5]. Enterprise Wi-Fi systems deployed in stadiums and airports etc. use the AP controller to control the transmission power, assign or modify the channel numbers to overcome co-channel or adjacent channel interferences among co-existing APs. Wi-Fi area simulation tools [13] can help to determine how many APs are necessary and where deploy the APs to cover a certain place. The tool and other enterprise level centrally controlled Wi-Fi systems take consideration of the relation between APs to provide Wi-Fi coverage.

However, the above Wi-Fi AP deployment methods cannot be applied to MAPs deployment in PCoHST because of the following problems.

Problem 1. Traditional 2.4GHz or 5GHz band Wi-Fi systems do not suffer from the path loss degradation as severe as mmWave band, so the LOS or NLOS relation of each AP and each UT was not taken into full consideration in the lower frequency bands. But the free space path loss at 60GHz is about 28dB bigger than that of 2.4GHz, therefore, the LOS and NLOS relation between the MAPs and the UTs cannot be ignored in the 60GHz band.

Problem 2. Wi-Fi deploy methods do not take full consideration of the degradation due to human blockage because at 2.4GHz it is relatively small, up to about 10dB in the full blockage scenario [14]. But the degradation due to human blockage can be up to 35dB in 60GHz band [10], i.e., 25dB severer than the 2.4GHz band so it shall be considered.

Problem 3. The antenna adopted in Wi-Fi deploy methods usually are either Omni antenna or directional antenna with wide beam width. But these antennas can no longer support enough coverage in mmWave band due to the larger path loss and severer human blockage. Therefore in mmWave band high gain beamforming antenna with narrow beam width are necessary to enhance the mmWave coverage.

### C. Points to Ponder for MAPs Deployment

This subsection addresses the following 3 points need to be pondered from the perspective of MAPs deployment. Point 1 and Point 2 arise from the 3 problems listed in Section II-B when trying to apply the Wi-Fi AP deployment methods to MAPs deployment. Point 3 originates from the need to satisfy the mmWave coverage in the PCoHST by 4 MAPs.

Point 1. In order to solve Problem 1 and Problem 2 in Section II-B in 60GHz band, i.e., bigger path loss and severer human blockage degradation, the LOS and NLOS relations between each MAP and UT at every seat and the relative position of the standing passengers to each MAP and UTs should be considered. Otherwise the coverage of one MAP may differ greatly due to the positions of the MAP.

Point 2. The antenna with sharp beams for both the MAPs and UTs shall also be considered corresponding to Problem 3 in Section II-B. Otherwise, the mmWave coverage of one MAP is small, and hence more than 4 MAPs will be required.

Point 3. How to deploy the 4 MAPs so that the UTs at all the seats in the PCoHST are in the mmWave coverage? Besides the above Point 1 and Point 2, the load of each of the 4 MAPs shall be properly balanced so that every MAP can provide gigabit class mmWave coverage to about 25 seats with strong enough LOS and NLOS paths. And it is desirable for the UTs at those seats 2 or 3 seat rows apart from the seat row right beneath the MAP to have LOS relation or strong NLOS relation with at least one of the other 3 MAPs. Otherwise the RSSI at those UTs may drop below -64dBm and cannot provide Gigabit level link throughput especially when the communicating path between an MAP and a UT becomes degraded by human blockage.

## II. EVALUATION METHODS, THE TATS AND THE HUMAN BLOCKAGE ISSUES AND SIMULATION PARAMETERS

This section comprises of 4 parts. We first introduce the evaluation methods in Section III-A. Then, we explain the following simulation parameters: the two proposed TATs as well as 10 TATs for comparison in

Section III-B; human blockage issues in Section III-C; and the other simulation parameters in Section III-D.

A. Evaluation Methods

We investigate where to deploy the 4 MAPs by the following 3-step evaluation methods.

Step 1: Propose TATs for the 4 MAPs based on the 3 points of pondering for MAPs deployment in Section II-C.

- 1) In order to cope with Point 1 in Section II-C, propose the TATs that are potential to provide as many as possible LOS relation between the MAPs and UTs and achieve strong NLOS paths for other seats even when some passengers are standing. The suitable position of each MAP shall be investigated from possible choices in both the direction of sleeper and the travel direction, such as at or close to the center of the vehicle width, or over each seat of a certain seat row (please refer Section III-B for detail seat arrangement in the PCoHST) up to the ceiling or luggage rack in the direction of the sleeper, and the ceiling between seat rows or the terminal wall above or near the automatic door in the travel direction.
- 2) Point 2 in Section II-C has been reflected in Section II-A as the second premise of the simulation so that it is used as common parameter for evaluating all the TATs.
- 3) In corresponding to Point 3 in Section II-C, all the 4 MAPs should be evenly or quasi-evenly distributed with a proper interval in the travel direction of the train.

Step 2: Evaluate the performance of each TAT by changing the parameters in Section III-B, Section III-C and Section III-D one by one to calculate the RSSI of UTs at each seat for each TAT so as to find TATs that can satisfy the at least 99% coverage target. In detail, locate the MAPs according to each TAT, set the antenna pattern and then calculate the RSSI at every seats in the PCoHST by simulation considering the human blockage degradation of both sitting and standing passengers under 4 typical human blockage scenarios and 3 typical occupancy rates.

Step 3: Compare the performance of the proposed TATs with the other possible types in terms of the cumulative distribution function (CDF) of RSSI and mmWave coverage rate. The TATs that can achieve at least 99% coverage rate target are feasible allocation types.

B. The Topographic Allocation Types

First, this subsection states the key point of the evaluation, i.e. the TATs used in the computer simulations. The layout of the PCoHST is introduced before the TATs.

- The layout of the PCoHST:

The PCoHST for our simulations is the ordinary 100-seat passenger car of a high speed train [3]. As shown in Fig. 1 (a) and (b), the ordinary car is 21,410mm long and filled with 20 rows of seats. The seat arrangement of each

row is 2 and 3 connected seats, separated by the aisle, hence each car can accommodate up to 100 passengers. The (X, Y, Z) coordinates of the PCoHST is illustrated in Fig. 1. The other cross-section views of the ordinary type passenger car and the side view of the seat can be found in [3].



Fig. 1 (a). A top view of the 100-seat ordinary type car

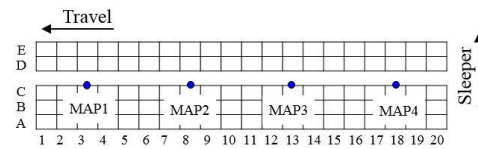


Fig. 1 (b). A cross-section drawing of the ordinary type car

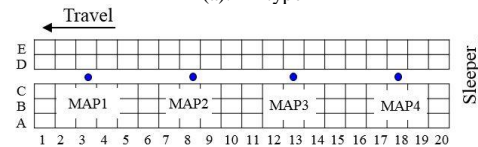
- Some topographic allocation types

From the perspective of MAPs allocation, and taking consideration of the layout of the PCoHST as in Fig. 1 and other figures in literature [3], we propose the following I-1 type and I-2 type as shown in Fig. 2 because they can provide more balanced LOS paths and stronger NLOS paths between the MAPs and the seats.

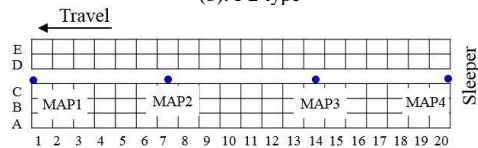
The TATs can be classified into the following two categories: I-category and N-category. Fig. 2 and Fig. 3 respectively depicts some I-category and N-category TATs. The category name is taken from the letter formed by connecting the adjacent MAPs of the top view figure of the PCoHST. I-category TATs are viewed from the travel direction of the PCoHST, while the N-category ones are viewed from the both the direction of the railway sleeper and the travel direction. It is impossible to set up antenna poles for the MAPs inside the PCoHST because the poles will not only bring troubles for the passengers in motion but also affect the beauty of design. So the MAPs are needed to be imbedded either in the wall, in the ceiling, or in the luggage rack above the seating height of the passengers so as to achieve as many as possible LOS relation between at least one MAP and the UTs.



(a). I-1 type



(b). I-2 type



(c). I-3 type

Fig. 2. Three I-category TATs

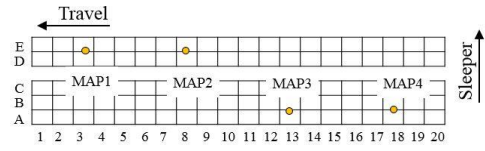
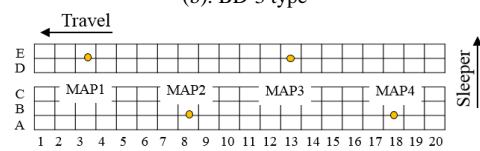
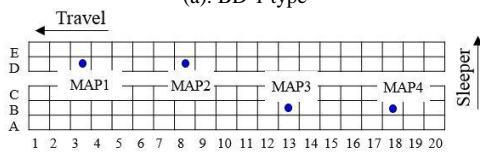
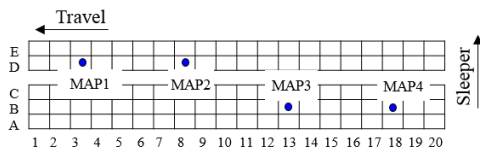
I-1 type and I-2 type as shown respectively in Fig. 2 (a) and Fig. 2 (b) are proposed in order to find the proper positions for the MAPs to satisfy the mmWave coverage target in the PCoHST with 4 MAPs. The 4 MAPs of I-1 type and I-2 type are evenly allocated in the direction of moving to the ceiling along the center of vehicular width and that of the aisle width so that each MAP can have almost the same number of LOS UTs and balanced number of strong NLOS UTs. In order to guarantee the RSSI of the UT at any seat is strong enough for gigabit class link throughput, both the LOS and NLOS relation between MAPs and UTs are considered besides the TX/RX beam gain, beam direction, and the transmission power. I-2 type differs from I-1 type in that the Y axis positions are at the center of the aisle width instead of the center of the vehicular width.

The candidate positions of MAPs, (X, Y, Z) for all the TATs are chosen based on the considerations of MAPs deployment. For instance, Table I lists the set of the typical X axis positions of the 4 MAPs of I-1 type as shown in Fig. 2 (a). For I-1 type,  $Y=0$  and  $Z=2090\text{mm}$  because the 4 MAPs are attached to the ceiling along the center of the vehicular width of PCoHST.

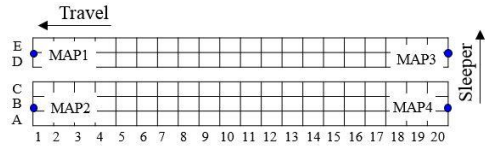
TABLE I: TABLE OF MAP POSITIONS

Number of MAPs	X-axis positions of MAPs in the travel direction (mm)			
	MAP1	MAP2	MAP3	MAP4
4	2676	8028	13381	18733

I-3 type as depicted in Fig. 2 (c) is one of the allocation options of the 4 MAPs. Like I-1 type, the 4 MAPs of I-3 type are also evenly allocated to the ceiling along the center of aisle width, but I-3 type differs from I-1 type in that the X-axis positions as shown in Fig. 2 (c) and Fig. 2 (a): the MAP1 and MAP4 of I-3 type locate at the both ends of the PCoHST above the front and back gates, while MAP2 and MAP3 at the 7th and 14th seat row respectively. The distance between two adjacent MAPs of I-3 type is about 7137mm and that of I-1 type is about 5353mm.



(d). AE-3 type



(e). T2T2 type

Fig. 3. Five of the nine N-category TATs. Blue MAPs: 2m, Yellow MAPs: 1.6m.

Fig. 3 shows 5 of the 9 N-category TATs for the 4 MAPs. Fig. 3 (a) and Fig. 3 (b) show that 4 MAPs are evenly distributed along the travel direction and are allocated to the ceiling (2090mm high) alternatively above certain B seats and certain D seats in the direction of the railway sleeper. Fig. 3 (c) and Fig. 3 (d) show that 4 MAPs are evenly allocated along the travel direction to the bottom plane of the luggage rack (1600mm high) alternatively above certain A seats and certain E seats along the sleeper. The positions on the X axis, i.e., the travel direction of the train are the same as those in Fig. 2 (a). Fig. 3 (e) shows that T2T2 type where the 4 MAPs are allocated to the ceiling at both ends of the PCoHST above the doors.

C. Human Blockage Issues

Next, this subsection treats human blockage issues that greatly affect the mmWave propagation characteristic inside the PCoHST. Human body model used in the simulation is introduced before the 4 human blockage scenarios.

- Human body model and human skin parameter: The size for passengers on the train is based on the human size data [15] by METI (Ministry of Economy, Trade and Industry of Japan). The permittivity of the human skin is referred from the corresponding mmWave band data [16].
- 4 human blockage scenarios:

We classified human blockage scenarios into the following 4 based on the statistics of passenger boarding rate in the PCoHST [17]. In the following human blockage scenarios, we assume that every passenger sits in his/her seat in the PCoHST except those who stand in the PCoHST.

Scenario 1: when the boarding rate is more than 120% during the busy holiday seasons [17] up to 20 passengers stand on the aisle. We assume that they are standing on the aisle near the C seats, one person per seat row.

Scenario 2: Some passengers are waiting in line along the aisle before getting off at a midway station. For this scenario, we assume that 10 passengers are waiting and 5 passengers near each of the two gates of the PCoHST.

Scenario 3: Several passengers are standing between two adjacent rows in front of or behind a certain seat row,

e.g. in the scene that some passengers are putting their luggage on the luggage rack after boarding the PCoHST. We assume that 6 passengers are standing, 3 in front of and the other 3 right behind the target seat row.

Scenario 4: every passenger in the PCoHST is sitting in his/her seat and there is no person on the aisle.

The occupancy rate and the boarding rate in the PCoHST are respectively defined in Eq.1.

$$\text{Occupancy rate} = \frac{N_{os}}{N_s} \tag{1}$$

$$\text{Boarding rate} = \frac{N_p}{N_s} = \text{Occupancy rate} + \frac{N_{ss}}{N_s}$$

where  $N_{os}$  is the number of seats occupied by passengers,  $N_s$  is the total number of seats,  $N_p$  is the number of all total number of passengers in the PCoHST and  $N_{ss}$  is the number of standing seats in the PCoHST.

Besides the most severe case in Scenario 1, where 20 passengers standing on the aisle, corresponding to the 120% boarding rate in the PCoHST, the statistical passenger boarding rate 100%, 80% and 60% [15] are also considered. When the boarding rate is below 100%, everyone can take a seat, so the above Scenario 1 does not exist. If there is no standing seats then boarding rate equals to occupancy rate. So for the sake of brevity, hereinafter occupancy rate is mainly used to emphasis the sitting pattern.

We assume that all the D seats are vacant when the seat occupancy rate is 80%, and that all the B and D seats are vacant when the seat occupancy rate is 60%.

**D. Other Simulation Parameters**

Finally, this subsection states some other simulation parameters besides those described in previous sections, as well as how the RSSI of the UTs are simulated.

- The dielectric parameters of the floor, walls, ceiling, luggage racks, seats etc.:

The parameters are based on ITU-R P.1238-7 [18]

- Transmission power of the MAPs and UTs:  
10mW is adopted following the Radio Regulation of Japan.

- Antenna of the MAPs and the UTs:

The antenna of each MAP or UT is an 8 by 8 directional beam switching antenna as shown in Fig. 4 (a). The half power bandwidth (HPBW) of the MAPs and the UTs are respectively set as 15 and 60 degree. The 3D pattern of the antenna beam is illustrated in Fig. 4 (b). The gain of the each antenna beam of the MAPs and UTs is respectively about 21.8dBi and 11dBi. The HPBW of antenna beam of the UTs is set as 60 degree so that the RX antenna can receive multiple paths.

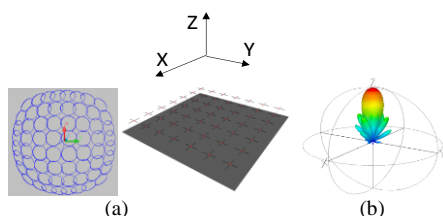


Fig. 4. Antenna pattern and beam direction

The directive pattern of each beam is shown in Eq. 2.

$$G(\theta) = \left( \frac{\sin a\theta}{a\theta} \right)^b \tag{2}$$

$$a[\text{rad}^{-1}] = \frac{131.8}{Bw[\text{deg}]}$$

where Bw stands for the 3dB beam bandwidth and b=3.

- Number of reflection and diffraction paths:  
NLOS paths exist for most of the seats. The NLOS paths comprise of both the reflected and diffracted waves. Besides the LOS path, up to 8 time reflection/diffraction or a combination of reflection and diffraction paths are calculated during the raytracing simulations.

- How to simulate the RSSI of the UTs

During the computer simulation, the RSSI for each receiving location of the UTs at every seat in the PCoHST is determined as the maximal one among the 4 MAPs. The RSSI from each MAP is calculated by applying every beam of the UT to all the transmitting beams of the MAP considering the beam gain, as well as the azimuth and elevation angles of each beam. The pair of TX beam of the MAP and the RX beam of the UT that leads to the maximal receiving power at the UT is adopted as the RSSI of the MAP.

For each seat, the observation or the receiving area of the mmWave enable UTs is 50cm by 50cm square and there are 4 by 4 evenly distributed observation planes, as shown in Fig. 5. The RSSI of each observation plane is chosen as the maximal RSSI from all the MAPs. At each seat, both the minimal and median RSSI of all the 16 observation planes are calculated. The better the RSSI distribution above the RSSI threshold at each seat, the more likely the TAT bring higher performance.



Fig. 5. An example of observation planes at each seat

The evaluation objects are each of the TAT, and the minimal and median RSSI of all the 16 observation planes.

The main evaluation criterion is the median of RSSI at multiple (i.e., 16) points shown in Eq.3:

$$\text{Median (RSSI}(i)) \geq -64\text{dBm}, i=1,2,\dots,16 \tag{3}$$

**III. SIMULATION RESULTS AND DISCUSSIONS**

This section summaries the simulation results corresponding to the 3 problems described in Section II-C. The results of Problem 3 is not shown separately because the solution of it has been reflected as the narrow antenna beam in simulation parameters. The following subsections first show that the proposed TATs, taken into consideration of the LOS and NLOS relation between the MAPs and the UTs in Section IV-A, and both the sitting and standing human blockage degradation in Section IV-

B, bring better performance under all the 4 typical human blockage scenarios. We further show that the performance difference of the TATs due to occupancy rates in Section IV-C before summaries and discussions in Section IV-D.

A. Performance Difference of the TATs Due to the LOS and NLOS Relations between the MAPs and UTs.

Table II shows the simulation results of 12 different TATs under the 4 typical human blockage scenarios defined in Section III-C when the occupancy rate is 100%. The 4 columns at left are respectively the condition in terms of the view direction, category and type the MAPs as well as the height of the MAPs. The 4 columns at right are the simulation results corresponding to the 4 scenarios in terms of the number of seats where the link throughput is below 1Gbps. The smaller the number, the better the performance.

TABLE II: PERFORMANCE OF THE 12 TATs UNDER 4 SCENARIOS

Occupancy rate=100%				Number of seats where link throughput is below 1Gbps			
View of direction	Category of TATs	Type of TATs	Height (m)	Human blockage scenarios			
				1	2	3	4
Moving	I	I-1	2.0	0	0	0	0
		I-2		0	0	0	0
		I-3		15	10	7	5
Vehicular width	N	BD-1	2.0	0	0	1	0
		BD-2		3	3	1	0
		BD-3		0	2	1	0
		BD-4		3	0	1	0
		AE-1	1.6	9	6	5	4
		AE-2		14	9	3	4
		AE-3		11	8	2	3
		AE-4		11	7	3	4
		T2T2		2.0	69	69	59

The 12 values under the each of the 4 human blockage scenarios in Table II show the performance of the corresponding TAT from the viewpoint of the LOS and NLOS relations between the MAPs and UTs. Table II shows that the performance of those TATs taking consideration of the relations, such as I-1 and I-2 type, are better than those not taking enough consideration of the relations such as I-3 type and T2T2 type. For example, under Scenario 1 in Section III-C, the number of seats below 1Gbps for I-1 and I-2 type is 0, while that for I-3 type (which takes some consideration of the LOS and NLOS relations) is 15, and that for T2T2 type is 69.

B. Performance Difference of the TATs from the Viewpoint of Sitting and Standing Human Blockage

For each of the 12 TATs in Table II, the right 4 columns under the 4 scenarios show the performance difference of the TAT from the viewpoint of sitting and standing human blockage. As stated in Section III-C, the number of standing passengers for Scenario 1, Scenario 2, Scenario 3 and Scenario 4 is respectively 20, 10, 6 and 0. Results in Table II show that the more the number of standing passengers, the more likely the number of seats below the mmWave coverage target. For example, the

number of seats below 1Gbps for I-3 type under the 4 human blockage scenarios is respectively 15, 10, 7 and 5. This is because the about 7136mm distance between adjacent MAPs of I-3 type is too large to cover the degradation to those NLOS UTs more than 3m apart from the MAPs due to the standing and sitting human blockages.

Fig. 6 shows the bar graph simulation results of 4 human blockage scenarios of the three ‘‘I’’ type TATs depicted in Fig. 3 and summarized in Table II when the occupancy rate is 100%. As shown in Fig. 6 for all the 4 human blockage scenarios, the mmWave coverage rates of I-1 type and I-2 type are all 100%, satisfying the at least 99% coverage target, while the coverage rates of I-3 type for the 4 scenarios are respectively 85%, 90%, 93% and 95%, failing to satisfy the coverage target.

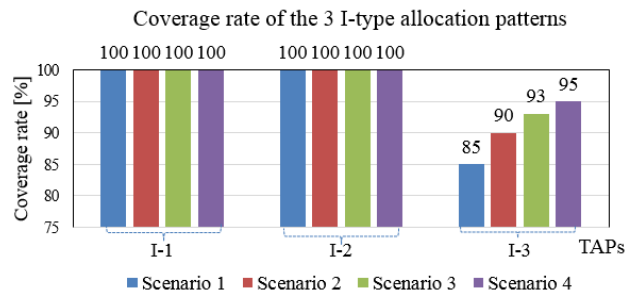


Fig. 6. Performance of the 3 I-category TATs

C. Performance Difference Due to Occupancy Rates

Scenario 1 is chosen because it is the most severe human blockage scenario where 20 passengers stand on the aisle. When the occupancy rate is respectively 100%, 80% and 60%, the boarding rate is respectively 120%, 100% and 80%. (Fig. 7)

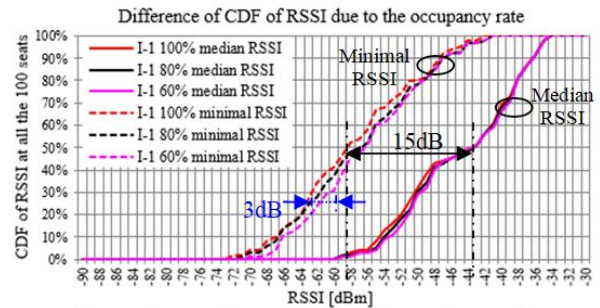


Fig. 7. Performance difference due to the occupancy rate

The three solid curves at the right side are the median RSSI, while the three dotted curves at left are the minimal RSSI among the 16 observation planes of each seat. The results show that although the minimal RSSI and median RSSI differs about up to 15dB, the difference due to the occupancy rate is less than 3dB. Furthermore, human body blockage at the sitting posture to the observation plane is not as severe as the standing posture.

The results corresponding to Table II when the occupancy rate is respectively 80% and 60% are omitted here for the sake of brevity and space. The conclusions

are that all the 4 BD type TATs also satisfy the RSSI criteria besides I-1 type and I-2 type.

Occupancy rate and human postures also affect the performance, and the standing posture causes worse influence to the RSSI value of the UT than the sitting posture.

D. Summaries and Discussions

This section first summarizes and then discusses the above simulation results in Section IV-A, Section IV-B and Section IV-C.

This paper investigates where to allocate 4 MAPs so as to achieve the at least 99% gigabit class coverage rate in the PCoHST. We proposed I-1 type and I-2 type and evaluated their performances together with 10 other TATs. Fig. 8 summarizes the performance of the proposed I-1 type, I-2 type and other types by the CDF of the RSSI at the 100 seats of the PCoHST with the human blockage Scenario 1 in Section III-C (the busiest scenario). The performance curves of BD-3 type, BD-4 type, AE-3 type and AE-4 type are omitted for the sake of brevity because they are similar to the corresponding performances of BD-1 type, BD-2 type, AE-1 type and AE-2 type.

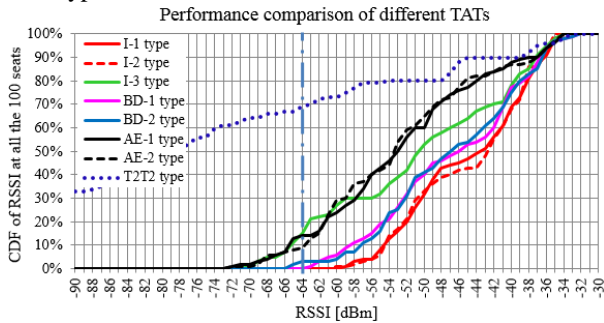


Fig. 8. Performance difference of different MAP TATs

Any TAT whose CDF performance is less than 1% when RSSI=-64dBm satisfy the coverage target, gigabit class link throughput at almost all (at least 99% of) the 100 seats. Fig. 8 shows that the RSSI at each of all the 100 seats in I-1 type, I-2 type and BD-1 type meet the coverage target. Furtherly Table II shows that only I-1 type, I-2 type can meet the target at 100%, and BD-1 type meet the target at 99%. Reviewing all the results in Fig. 8, for all the 4 human blockage scenarios and all the 3 occupancy rates and among the 12 types, the proposed I-1 type and I-2 type satisfy the link throughput target better the other 10 TATs.

Discussions of all the above simulation results are carried out from the viewpoint of the relation of performance the TATs and the distance between 2 adjacent MAPs in both the travel direction and the sleeper direction.

In order to guarantee that there is not more than 1 seat at which the link throughput is below 1Gbps, the MAPs need to be deployed with adequate intervals in the travel direction so that there is at least one strong LOS or NLOS path to almost every seat in the PCoHST. Simulation

results show that evenly distributed TATs with suitable intervals between adjacent MAPs such as I-1 type and I-2 type are fine while the non-evenly distributed type like T2T2 fails. Although I-3 type is also evenly distributed, but the about 7.1m interval of I-3 type is too large to provide strong LOS or NLOS path to some seats 2 or 3 rows apart from the MAPs.

Then in the sleeper direction, although AE-1 type and AE-2 type can provide stronger LOS path to some of the window side A or E seats but they cause weaker LOS and NLOS path to some other seats, hence unbalanced and worse performances. I-1 type allocated at the center of vehicle provide strong and balanced LOS or NLOS path to all the seats. As shown in Fig. 8, the order of the performances of I-1 type, I-2 type, BD-1 type, BD-2 type, AE-1 type and AE-2 type is listed in Eq. 4:

$$I-1 > I-2 > BD-1 > BD-2 > AE-1 > AE-2 \quad (4)$$

While the order of the distance from the MAPs of the corresponding TATs in Fig. 3 to the center of the vehicle is listed in Eq. 5:

$$AE-1(=AE-2) > BD-1(=BD-2) > I-2 > I-1 \quad (5)$$

Eq. 4 and Eq. 5 indicate that the farther away the MAPs are from the center of the vehicle, the worse the performance of corresponding TAT.

Therefore, the proposed I-1 type and I-2 type are better TATs than the others types because they have the above topographical allocation advantages in both the travel and sleeper direction, and the intervals between two adjacent MAPs are also proper. Moreover, as confirmed in the above summaries and discussions, the MAPs in I-1 type can offer more balanced LOS and NLOS relations with the A and E seats than I-2 type. Overall, I-1 type gives better RSSI performance in all the 4 typical human blockage scenarios regardless of the 3 different occupancy rates.

IV. CONCLUSIONS AND FUTURE WORKS

This paper proposed and evaluated the TATs of the MAPs taking into consideration of the physical layout of the PCoHST, the propagation characteristics of mmWave and obstruction of both standing and sitting human postures in 4 typical human blockage scenarios in PCoHST and 3 occupancy rates by a ray-tracing method.

The results show that the two straight in-line types, I-1 type and I-2 type, with the MAPs on the ceiling above the aisle give better RSSI performance than the other 10 TATs. Boarding rate and human body blockage also affect the performance, and the standing human body posture causes worse influence to the RSSI value of the UT than the sitting posture. Over all, I-1 type gives better RSSI performance in all the 4 typical human blockage scenarios regardless of the occupancy rates.

Further works include testing and evaluating the TATs in actual PCoHST.

ACKNOWLEDGMENT

This research is part of the research and development project “Millimeter wave backhaul technologies for high speed trains” funded by MIC of JAPAN.

REFERENCES

[1] H. Song, *et al.*, “Millimeter-wave network architectures for future high- speed railway communications: Challenges and solutions,” *IEEE Wireless Comm. Mag.*, vol. 24, no. 6, pp. 114-122, 2016.

[2] P. T. Dat, A. Kanno, N. Yamamoto, and T. Kawanishi, “WDM RoF-MMW and linearly located distributed antenna system for future high speed railway communications,” *IEEE Comm. Mag.*, vol. 53, no. 10, pp. 86-94, 2015.

[3] T. Endo, S. Tanaka, and H. Saito, “The E5 series shinkansen rolling stock of east Japan railway company (JR EAST),” *Rolling Stock Technology*, no. 241, pp. 3-28, March 2011.

[4] IEEE STD 802.11ad-2012.

[5] J. Moreno, M. Domingo, L. Valle, J. R. Perez, R. Torres, J. Basterrechea, “Design of indoor WLANs,” *IEEE Antenna & Propagation Magazine*, pp. 22-33, 2015.

[6] T. Hikage, M. Shirafune, T. Nojima, W. Yamada, and T. Sugiyama, “Numerical estimations of the propagation characteristics of wireless links in high-speed train cars,” in *Proc. International Symposium on Antennas and Propagation*, 2012.

[7] M. Shirafune, T. Hikage, T. Nojima, M. Sasaki, W. Yamada, and T. Sugiyama, “Propagation characteristic estimation of 5GHz-band wireless links in high speed train cars using FDTD Analysis,” *IEICE-B*, vol. J97-B, no. 9, pp. 762-789, 2014.

[8] N. Kita, T. Ito, S. Yokoyama, M. C. Tseng, Y. Sagawa, M. Ogasawara, and M. Nakatsugawa, “Experimental study of propagation characteristics for wireless communications in high-speed train cars,” in *Proc. European Conference on Antennas and Propagation*, 2009, pp. 897-901.

[9] T. Sugo, M. Hayashi, T. Maeyama, S. Imata, N. Suzuki, and S. Watanabe, “Propagation of wireless LAN in the train,” *IEICE Tech. Rep.*, vol. 113, no. 34, pp. 59-64, May 2013.

[10] M. Peter, M. Wisotzki, and M. Raceala-Motoc, “Analyzing human body shadowing at 60GHz: systematic wideband MIMO measurements and modeling approaches,” in *Proc. 6th European Conference on Antennas and Propagation*, March 26–30, 2012, pp. 468-472

[11] L. Rakotondrainibe, Y. Kokar, G. Zaharia, and G. El Zein, “Millimeter-wave system for high data rate indoor communications,” in *Proc. International Symposium on Circuits and Systems*, July 9-10, 2009.

[12] F. Lu, K. Yunoki, and N. Suzuki, “Influence of human body movement on mmWave communication in bullet train cars,” in *Proc. IEEE ICUBW’2016*, Oct. 2016.

[13] [Online]. Available: [http://www.ntt-at.co.jp/product/docs/Wifielder\\_161109.pdf](http://www.ntt-at.co.jp/product/docs/Wifielder_161109.pdf)

[14] The Human Body Blocks 2.4 GHz Signal. [Online]. Available:

<https://solahuddinyusuf.wordpress.com/2017/12/28/the-human-body-blocks-2-4-ghz-signal/>

[15] News Release of METI (Ministry of Economy, Trade and Industry, Size-JPN 2004-2006, Oct. 1, 2007.

[16] C. M. Alabaster, “Permittivity of human skin in millimeter wave band,” *Electron. Lett.*, vol. 39, no. 21, pp. 1521-1522, 2003.

[17] Boarding rate of Shinkansen. [Online]. Available: <http://www.shinkansen-yoyaku.com/congestion/jyousharitsu.html>

[18] Recommendation ITU-R P. 1238-7, “Propagation data and prediction methods for the planning of indoor radio communication systems and radio local area networks in the frequency range 900 MHz to 100 GHz,” 2012.



**Feng Lu** received Ph.D. in radio engineering from Beijing University of Posts and Telecommunications in 1996. He was a Postdoctoral Fellow at Kyushu University, Japan before joining Kyocera DDI Institute of Future Telecommunications, Inc. (now KDDI Research Inc.) in 1999. He is interested in wireless systems including millimeter wave as well as 5G and 5G beyond cellular system.



**Akira Yamaguchi** received B.S. and M.S. degrees in Electrical Engineering from Waseda University, Japan in 1989 and 1991, respectively. He joined KDD in 1991. He joined the Advanced Telecommunications Research Institute International (ATR) in 2005. He joined KDDI R&D Laboratories Inc. in 2008. His technical interests cover wireless system including millimeter wave, device-to-device communication, cellular system, dynamic resource allocation and cognitive radio. He is now with KDDI Research Inc.



**Kazunori Takeuchi** is the R&D manager of the Future Access Network Division at KDDI Research, Inc. Saitama Pref., JAPAN. Dr. Kazunori earned his BS, MS and Ph.D. degrees respectively from the Hokkaido University, Osaka University, and Waseda University, Japan. His main responsibilities was to proceed the project of Cognitive Radio Communication Technical Research funded from the Ministry of Internal Affairs and Communications (MIC) of Japan. He joined TOYOTA InfoTechnology Center for several years. He is also interested in the ITS as one of good application of the cognitive radio. He is also interested in the wireless applications including power transmission etc.



**Hiroyuki Shinbo** received the B.S. degree from University of Electro-Communications (UEC, Japan) in 1997, and the M.S. degree from the graduate school of information systems of UEC in 1999. He entered KDD Co. Ltd. (now KDDI Corporation) in 1999, and he has been the senior manager of smart

wireless technology development laboratory in KDDI Research, Inc. from 2016. His research interest includes the overall of mobile communication (including 5G and beyond, LPWA), TCP/IP and network management.